

THE PENNSYLVANIA STATE UNIVERSITY
SCHREYER HONORS COLLEGE

DEPARTMENT OF ENGINEERING SCIENCE AND MECHANICS

MAGNESIUM ALLOYS FOR USE IN BIOABSORBABLE CARDIAC STENTS

JACQUELINE G. VAN PELT

Fall 2009

A thesis
submitted in partial fulfillment
of the requirements
for a baccalaureate degree
in Engineering Science
with honors in Engineering Science

Reviewed and approved* by the following:

Barbara A. Shaw
Professor of Engineering Science and Mechanics
Thesis Supervisor

Christine B. Masters
Assistant Professor of Engineering Science and Mechanics
Honors Adviser

Judith A. Todd
P. B. Breneman Department Head Chair
Professor, Department of Engineering Science and Mechanics

* Signatures are on file in the Schreyer Honors College and Engineering Science and Mechanics Office.

Abstract

First introduced clinically in 1987, cardiac stents have become the standard of care for the treatment of coronary artery disease. Current materials used in cardiac stents were designed for their biocompatibility, mechanical properties, and corrosion resistance. The benefits of stenting are realized within the first few months after deployment and after that time, the stent presents an inflammation and vessel obstruction hazard. For these reasons, a stent made from a biocompatible alloy that will corrode and bioabsorb into the body at a controlled and uniform rate would maximize the benefits of cardiac stenting while minimizing complication risks. Magnesium alloys seem the most promising material prospect due to the biocompatibility and high reactivity of magnesium (although this may be too high). Polarization resistance and electrochemical impedance spectroscopy experiments in a simulated body solution (Hank's Balanced Salt Solution) were performed on existing magnesium alloys AZ31, AZ61, and AZ91 as well as innovative non equilibrium electron beam vapor deposit magnesium alloyed with titanium and yttrium. From these tests, the corrosion properties of the alloys could be evaluated. The AZ series of alloys have already been used with success as biomedical implants in clinical trials, but the presence of aluminum in the alloys remains a significant concern. The electron beam vapor deposited magnesium alloys allow higher concentrations of alloying elements in the material (which will lower the corrosion rate of magnesium) and may be the best candidate to perfect for use in bioabsorbable cardiac stents.

Table of Contents

Acknowledgments	iii
Chapter 1 – Introduction	1
Chapter 2 - Literature Review	3
2.1 Metallic Alloys and Medical Implants.....	3
2.2 Corrosion as an Electrochemical Process.....	4
2.3 Biodegradable, Metallic Cardiac Implants.....	6
2.4 Magnesium and the Human Body.....	7
2.5 Corrosion and the Human Body.....	9
2.6 Design Considerations.....	9
2.7 Magnesium and Corrosion.....	10
2.8 Prospective Biodegradable Magnesium Alloys.....	12
Chapter 3 - Experimental Design and Methods	13
3.1 Background Information.....	13
3.2 Materials.....	14
3.3 Method.....	15
3.4 Polarization Resistance.....	17
3.5 Testing Parameters.....	18
Chapter 4 – Results and Discussion	20
4.1 Corrosion Rate Data.....	21
4.2 Experimental Analysis.....	25
4.3 Surface Photographs.....	27
4.4 Interpretation.....	31
Chapter 5 – Conclusions	33
5.1 Summary.....	33
5.2 Future Work Suggestions.....	34
Appendix A – Tools	35
Appendix B – Alloy Composition Analyses	36
References	39

Acknowledgments

I would like to express my appreciation to Dr. Barbara Shaw, Dr. Ela Sikora, and John Petrilli for their guidance, support, and patience throughout this project.

Chapter 1

Introduction

Cardiac stenting has become the standard in treatment of coronary artery disease (Levesque, 2008). However, cardiac stents currently in use are not without flaws. There are clear long term medical risks. Over time, stents may migrate or move out of place and tissue often grows over the stents (Dvorak, 2008). The result is that the stent ends up blocking the passageway it was designed to keep open. Designing a bioabsorbable metal alloy would employ the electrochemical properties of metals to allow patients to reap the maximum health benefit from stents while reducing the safety concerns and long term complication risks.

Bioabsorbable stents would support the vessel during the period of high risk for recoil and then corrode or dissolve within the human body in a predictable and uniform manner after its useful life is over. Over time, the stents would completely degrade eliminating the long term risks of traditional corrosion resistant stents. Bioabsorbable stents would be safer for patients, allow children with growing arteries to be treated more safely, allow physicians more flexibility in future diagnosis and treatment, and reduce health care costs. They would eliminate foreign material that may cause a thrombotic event. Unlike conventional stents, bioabsorbable stents would not interfere with the diagnostic evaluation of non-invasive imaging such as cardiac magnetic resonance and CT. They would eliminate the need for subsequent surgery for stent removal which is frequently done when in-stent restenosis, inflammation, or

stent migration occurs over time. This would reduce medical costs for cardiac patients.

The ultimate goal of the project is to design, develop, and test a bioabsorbable cardiac stent prototype made from a non equilibrium vapor deposited magnesium, titanium, and yttrium alloy. In this paper, the corrosion rates of traditional magnesium alloys AZ31, AZ61, and AZ91 in a simulated body environment were tested and compared with the corrosion rates of a non equilibrium vapor deposited magnesium, titanium, and yttrium alloy.

Chapter 2

Literature Review

2.1 Metallic Alloys and Medical Implants

Due to their superior mechanical properties such as stiffness and hardness, metallic alloys have long been used for a variety of medical implants. Other benefits of metals as medical implants include their visibility in x-ray images and the biocompatibility of many metals. Metallic alloys currently being widely used for medical implants in humans and a number of their applications are shown in Table 1. The image in Figure 1 illustrates the location on the human body of various medical implant devices and what metallic alloys are frequently used for those implants.

Material	Major Application
316L Stainless Steel	Cranial plates, orthopedic fracture plates, dental implants, spinal rods, joint replacement prostheses, stents, catheters
Cobalt-Chromium alloys	Orbit reconstruction, dental implants, orthopedic fracture plates, heart valves, spinal rods, joint replacement prostheses
Titanium, Nitinol, Titanium alloys (Ti-6Al-4V, Ti-5Al-2.5 Fe, Ti-6Al-7Nb)	Cranial plates, orbit reconstruction, maxillofacial reconstruction, dental implants, dental wires, orthopedic fracture plates, joint replacement prostheses, stents, ablation catheters

Table 1. Current biomedical metals and alloys and their applications (Hansen, 2008).

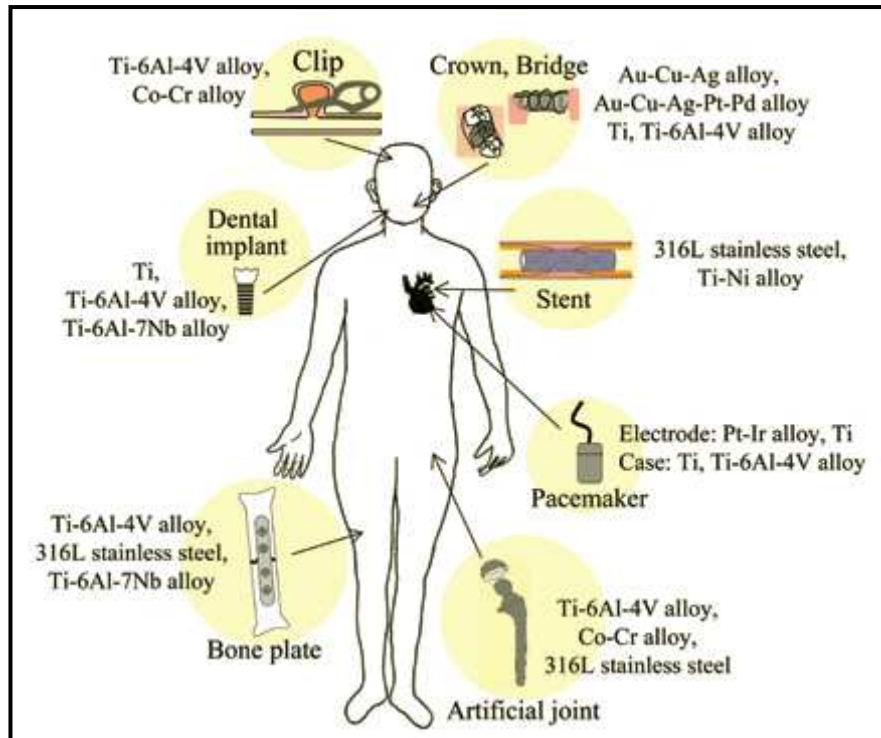
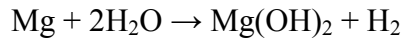


Figure 1. Metallic devices and the biomaterials used for them (Hiromoto, 2008).

2.2 Corrosion as an Electrochemical Process

The most significant drawback of metallic alloys is the electrochemical reactions that take place on the metal surface in the body (Schmutz, 2008). Corrosion is the destructive result of the chemical reactions between a metal or metal alloy and its environment and nearly always involves the transfer of electronic charge between the metal and components of a surrounding aqueous solution (Jones, 1996). The overall result of the electron transfer is an oxidation reduction reaction in which the metal loses electrons (is oxidized) in the anodic reaction and an element in the aqueous solution (frequently hydrogen) gains electrons (is reduced) in the cathodic reaction. The example overall reaction below represents corrosion of magnesium

through reaction with water. The cathodic and anodic reactions are also shown individually.



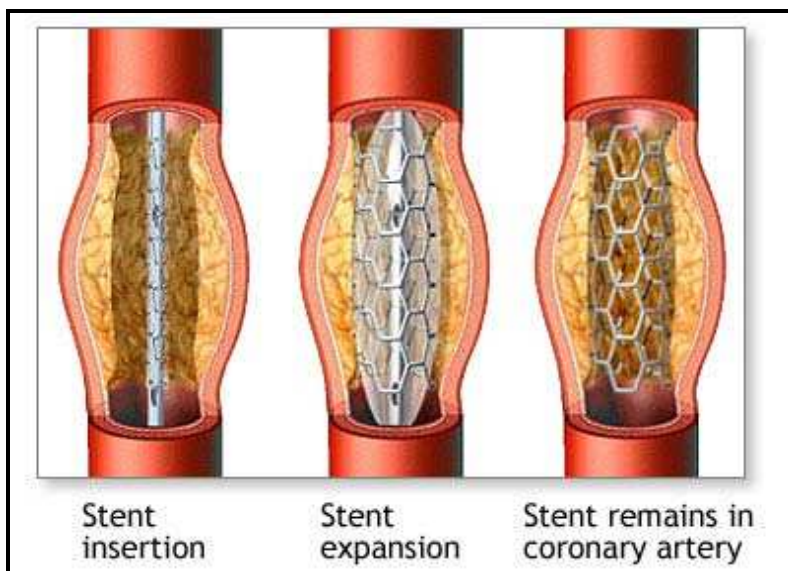
The electrons and oxidized metal ions that result from the anodic reaction migrate to the metal surface. Here, the metal dissolves as metal ions are liberated into the solution and electrons interact in the cathodic reaction and are carried away.

Corrosion is most commonly viewed as a detrimental process. In the United States alone, the direct economic costs of corrosion have been estimated between \$8 million and \$126 billion per year. Indirect costs also result from such sources as plant downtime to repair corroded equipment, loss of product from corroded containers that leak, loss of efficiency as a result of accumulated corrosion products in tubing or pipelines, contamination by soluble corrosion products, and overdesign because of ignorance or lack of the necessary corrosion information (Jones, 1996). As a result, the primary focus of corrosion science or the study of the chemical and metallurgical processes that occur during corrosion has been in designing and applying corrosion prevention methods. For this reason, the idea of bioabsorbable medical implants that would corrode within the body and subsequently disappear requires approaching corrosion from a new angle.

2.3 Biodegradable, Metallic Cardiac Stent Implants

Much research has recently been focused on using the electrochemical reactions of metals in a positive manner by developing biodegradable metallic implant materials. Such materials would need to corrode within the body at a uniform and controlled rate without releasing corrosion products of a size, type, or concentration that might pose a health threat to the individual. Development of a biodegradable metallic material would eliminate many long term complications of medical implants such as chronic inflammation, restenosis, and thrombosis (Waksman, 2007). Restenosis is the recurrence of constriction or narrowing of the diameter of a vessel. Thrombosis is the formation of a blood clot within a blood vessel. Bioabsorbable stents would also eliminate the need for follow-up surgeries to remove permanent devices. A biodegradable material may offer the ideal solution for cardiac stent implants.

Cardiac stents were introduced clinically in 1987 by Sigwart et al. who implanted a stent into humans after angioplasty for the purpose of supporting the blood vessel. From 2002-2003 more than half a million adult patients discharged from a hospital in the United States had at least one coronary stent insertion procedure performed (Levesque, 2008). Coronary stents are now the standard in care for patients with coronary artery disease. Figure 2 is an image demonstrating the process of how a traditional stent is used. The stent is inserted into the vessel in a compact form, expanded, and then remains in the artery to keep the vessel open.



<http://www.walgreens.com/library/graphics/images/en/19006.jpg>

Figure 2. Images demonstrating the use of a cardiac stent.

Permanent implantation of stents is unnecessary since the healing process of the occluded artery lasts at most between six months and one year (Levesque, 2008). After this time, the stent is no longer beneficial and instead presents health risks such as inhibiting the ongoing arterial healing process and provoking in-stent restenosis. A biodegradable stent would scaffold the vessel wall throughout the healing process and then degrade.

2.4 Magnesium and the Human Body

As a result of their extreme reactivity, magnesium alloys are excellent candidates for degradable implants. Furthermore, magnesium is biocompatible, present in large amounts in the body, and vital for metabolic processes and biological mechanisms (Schmutz, 2008 and Levesque, 2008). Magnesium has hypothrombogenic properties meaning that it has a low incidence of causing blood

clots that grow while remaining attached to the blood vessel wall and then pose a serious hazard of breaking loose and occluding smaller vessels. The predictable local tissue tolerance of corrosion and the expectation that corrosion products of magnesium would produce minimal adverse side effects are further evidence that magnesium is likely to be suitable as a degradable implant (Erne, 2006).

At least one laboratory in Europe has already developed stents made from magnesium alloys and tested them in clinical trials. There was between 3 and 6 mg of magnesium in prototype magnesium stents (estimation based on the stent length). Magnesium is the fourth most plentiful cation in the body and the release of this amount of magnesium over the course of several months during degradation of the stent should not cause tissue harm. The released concentrations of magnesium from the stent would be minimal in comparison to physiological plasma magnesium content of 0.70 to 1.05 mmol/L. Furthermore, the slow release of magnesium during stent degradation is expected to have beneficial effects since magnesium insufficiency in the body contributes significantly to cardiovascular disease. There is also sufficient evidence to support that magnesium serves as a systemic and coronary vasodilator, is involved in muscle contraction, is a cofactor of ATPase, and acts as a physiologic calcium antagonist (Erne, 2006). As such, magnesium prevents intracellular calcium overload in ischemia and platelet aggregation, reduces vascular resistance and increases the cardiac index (a measure of cardiac output by body surface area), and lowers systemic blood pressure. Additionally, magnesium alloy biodegradable stents are anticipated to offer the possibility for integration with local drug delivery, genetic transfer, and radiation.

2.5 Corrosion and the Human Body

The concept of biodegradable medical implants highlights the need for a better understanding and characterization of the interaction between metal surfaces and the surrounding physiological environment. The metal surface interaction of medical implants with the surrounding environment can lead to failure of the implant through degradation and corrosion which weaken the material and compromise its functionality. The human body environment contains water, complex organic compounds, dissolved oxygen, sodium, chloride, bicarbonate, potassium, calcium, magnesium, phosphate, amino acids, proteins, plasma, lymph, saliva etc. and can differ somewhat between individuals and over time within a single individual (Hansen, 2008). With body fluid at a temperature of about 98.6°F (37°C) and a buffered pH of around 7.4, the human body is not an entirely welcoming host (Hansen, 2008). When considering bioabsorbable medical implants, this corrosive interaction between metal and body is desirable after the functional life of the implant has concluded. Developing a deeper understanding of the corrosion interactions between metal alloys and the human body through *in vitro* and *in vivo* studies will allow metallic alloys to be engineered most precisely for specific medical implant applications.

2.6 Design Considerations

While design of a bioabsorbable stent material may offer the best clinical treatment for occluded arteries, the development of such a material breaks the

paradigm of corrosion resistant biomaterials and is not without challenges. There are many considerations in finding the optimal alloy composition including mechanical and corrosion properties and toxicity of alloy components. Among the mechanical properties to be considered are elasticity, ductility, elastic yield, and resistance to rupture.

The mechanical properties as a function of corrosion time are also important to consider. Ideally, the mechanical properties of the material would not be affected until after the healing process has been completed. Since patient safety is the number one design consideration with any medical device, ensuring that the corrosion process does not induce negative side effects on the patient's health is paramount. The corrosion products released throughout the degradation of the stent must not cause any toxic, carcinogenic, or mutagenic effects. Furthermore, the degradation process must not pose a vessel blockage hazard. To ensure that is the case, the alloy should corrode homogeneously without generating particles larger than a few microns. Ideally, the corrosion products would be no larger than the dimensions of capillaries (Levesque, 2008).

2.7 Magnesium and Corrosion

Magnesium is an excellent biodegradable stent material prospect because it is highly susceptible to corrosion. At the same time, research on magnesium corrosion offers some methods that could be used to increase and control the corrosion resistance of magnesium alloys to give them the corrosion properties desirable of bioabsorbable medical implants. Magnesium's atomic diameter of 0.320 nm makes it

a favorable size with a range of solute elements including aluminum, zinc, cerium, yttrium, silver, zirconium, and thorium (Song, 1999). Since magnesium is one of the lightest metals, magnesium alloys have high strength to weight ratios.

According to Song, the corrosion rate of magnesium is generally between that of aluminum and mild steel depending on the environment (Song, 1999). In most cases, the corrosion of magnesium alloys initiates from localized corrosion although the localized corrosion can be shallow and widespread. Magnesium alloys suffer more rapid corrosion in moist conditions and are susceptible to galvanic corrosion. However, metals with an active corrosion potential and a high hydrogen overpotential such as Al, Zn, Cd, and Sn do not cause as severe galvanic corrosion as metals with a low hydrogen overvoltage that constitute efficient cathodes for magnesium such as Ni, Fe, and Cu (Song, 1999).

Standard designation for magnesium alloys involves a combination of letters followed by numbers to indicate the composition of the alloy. In most cases, magnesium alloys are identified by two letters and two numbers. The first two letters identify the most important alloying components using the code designations shown in Table 2. The two digits that follow indicate the nominal concentrations of the principle alloying elements in percent by weight. For example, AZ31 is a magnesium alloy containing 3% aluminum by weight and 1% zinc by weight. There may be another letter following the numbers to differentiate an alloy from a series of alloys containing the same concentrations by percent weight of the primary alloying elements.

Letter Designation	Element or Elemental Group
A	Aluminum
E	Rare Earth
H	Thorium
K	Zirconium
M	Manganese
Q	Silver
S	Silicon
Z	Zinc

Table 2. Magnesium alloy standard designations.

Variations in metal alloy compositions can lead to differences in mechanical, physical, and electrochemical properties. Variations in fabrication methods, heat treatment, cold working, and surface finishing have an even more significant impact on corrosion and other properties of alloys.

2.8 Prospective Biodegradable Magnesium Alloys

There has already been progress in the development of degradable magnesium alloys. The potential for magnesium alloys as bioabsorbable stent material was confirmed with stent prototypes of AE21 implanted in pigs (Levesque, 2008). Stent prototypes of WE43 were recently preclinically implanted in lower limb ischemia in adult patients and used to treat congenital heart diseases in newborn babies (Levesque, 2008). Other magnesium alloys that have been cited in studies as promising candidates include AZ31, AZ91, LAE442, and AM60B (Levesque, 2008).

Chapter 3

Experimental Design and Methods

3.1 Background Information

Electrochemical techniques can be used to study corrosion since corrosion is an electrochemical process. In this way, *in vitro* corrosion testing of magnesium alloy samples was performed. The two corrosion tests performed on each sample were polarization resistance and electrochemical impedance spectroscopy, both of which yield a corrosion rate for the sample. All tests were conducted in Hank's Balanced Salt Solution (HBBS) at 37°C to simulate the environment and temperature within the human body. The HBSS used had the composition as shown in Table 3.

Component	Concentration (mg/L)
CaCl ₂ ·2H ₂ O	186
KCl	400
KH ₂ PO ₄	60
MgSO ₄	98
NaCl	8000
NaHCO ₃	350
Na ₂ HPO ₄ ·7H ₂ O	90
Glucose	1000

Table 3. Concentrations of Components of Hank's Balanced Salt Solution

HBBS is a simulated body fluid. However, the testing environment lacks a few important characteristics of the environment within the human body. The HBBS lacks proteins present in the body and in the testing environment the HBBS is stagnant as opposed to the movement of fluids within the body. The complexity of body fluid cannot be simulated exactly in the laboratory. Use of HBBS simulates the body environment while minimizing experimental variables and increases the reproducibility of the system. Even with these simplifications for *in vitro* experiments, the corrosion resistance ranking of the same biomaterials measured *in vitro* and *in vivo* are the same (Hansen, 2008).

3.2 Materials

Preliminary experiments were conducted on bulk samples of the following magnesium alloys: AZ31, AZ61, and AZ91. Results of the Materials Research Institute's composition analysis of the bulk samples used are shown below in Table 4.

Alloy	AZ31		AZ61		AZ91	
	ppm	% weight	ppm	% weight	ppm	% weight
Mg	685	95.389	1050	93.150	1350	90.253
Al	21	2.924	65	5.766	130	8.691
Zn	7.4	1.030	6.9	0.612	9.8	0.655
Na	2.2	0.306	2	0.177	2.6	0.174
Mn	2.1	0.292	2.7	0.240	2.8	0.187
K	0.29	0.040	0.32	0.028	0.38	0.025
Fe	0.09	0.013	0.23	0.020	0.14	0.009
Cu	0.02	0.003	0.02	0.002	0.02	0.001
Pb	0.01	0.001	0.04	0.004	0.05	0.003
Ni	< 01		< 01		< 01	
Sn	< 01		< 01		< 01	

Table 4. Composition of Mg Alloys by ppm and Weight Percentage.

The preliminary experiments established thresholds against which the primary experiments could be compared. Primary experiments were done using the non equilibrium vapor deposited alloys made from magnesium, titanium, and yttrium. The composition of all the samples of the materials used was analyzed by Henry Gong of the Materials Characterization Lab in the Materials Research Institute at Penn State University on a Perkin-Elmer Optima 5300 ICP machine. Complete results can be found in Attachment B.

3.3 Method

Bulk metal samples as used in preliminary experiments were encased in epoxy with only one flat metal surface exposed. First, copper tape was attached to the bulk sample to make an electric connection. The copper tape was covered with plastic tubing to protect the wire from exposure to HBSS during testing. The sample and connection with the plastic tubing were covered in epoxy. Air bubbles were removed from the epoxy by placing the sample in a vacuum desiccator. After the epoxy hardened, one side of the metal surface (parallel to the plastic tubing) was sanded until the metal surface was exposed and flat.

Thin and thick film samples made of vapor deposited alloys were prepared by attaching copper tape to the side of the surface and extending it a few inches off the sample to create a handle and a electrical connection to the metal. Black wax was then used to cover the edges of the sample and all of the copper tape contacting the metal as well as enough of the tape so that it would not be exposed to the HBSS during the experiment.

After sample preparation, surface area measurements of the exposed metal were taken and the testing environment was prepared. Approximately 100 mL of HBSS was placed in a beaker. A counter electrode (graphite rod) and reference electrode were placed in the solution and it was heated to 37 C. The sample was then placed in the solution until completely submerged while being careful not to allow the copper wire to contact the electrolyte. The exposed metal surfaces undergoing corrosion testing were vertical to minimize the buildup of hydrogen bubbles on the surface. Due to the length of the testing of the bulk metal samples, the beakers were covered to minimize evaporation and distilled water was added as necessary to maintain the electrolyte volume. The electrodes, sample, and thermometer were held in place using clamps, clips, and stands.

The system was connected to the computer testing equipment and polarization resistance (PR) and electrochemical impedance spectroscopy (EIS) tests were performed at regular intervals. The open circuit potential of the system was measured for between 100 and 300 seconds to ensure that it was in steady state prior to each test. For bulk samples in the preliminary tests, PR and EIS tests were performed once daily for the first seven days and once every three days for the remainder of the experiment. For the thick and thin film samples in the primary experiments, PR and EIS tests were run about once every two hours for the life of the samples. The samples eventually degraded to expose the silicon wafer or the black wax degraded exposing the copper wire. The samples were visually evaluated and the open circuit potential was monitored to determine when either of these events had occurred and then testing was concluded for that sample. Figure 4 shows images of the sample

surfaces under the microscope which reveal the types of sample degradation that occurred.

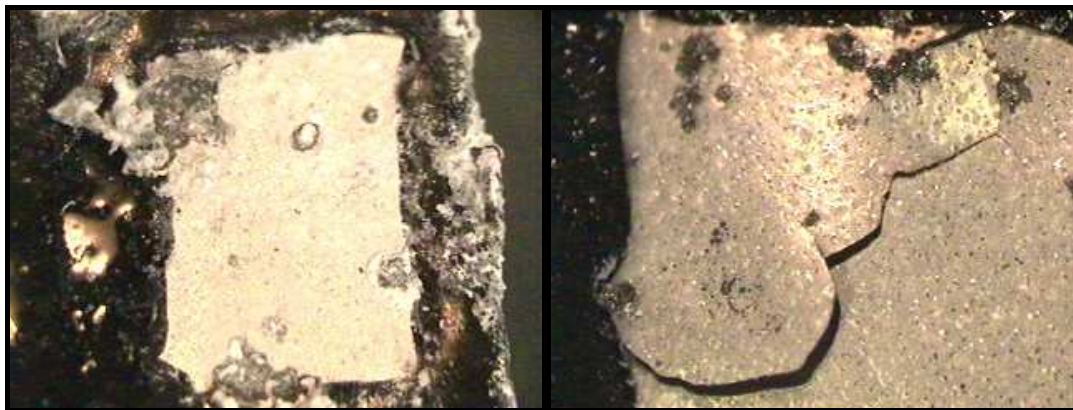


Figure 4. Testing was discontinued after the back wax degraded exposing the copper tape (left) or the film cracked or corroded exposing the silicon wafer base (right).

3.4 Polarization Resistance

Polarization resistance is a well accepted electrochemical method of determining corrosion rate. This method requires less time than the conventional weight loss method and does not require accelerating factors (such as increased temperature). Furthermore, polarization resistance is a nondestructive test so it can be repeated on the same sample over a period of time.

In the polarization resistance experiment, a current versus voltage curve is recorded as the cell voltage is swept over a small range of potential centered at the steady state potential of the corrosion cell. Figure 5 shows a screen shot of a polarization resistance curve and the line of best fit from which the R_p value was determined and the corrosion rate was calculated.

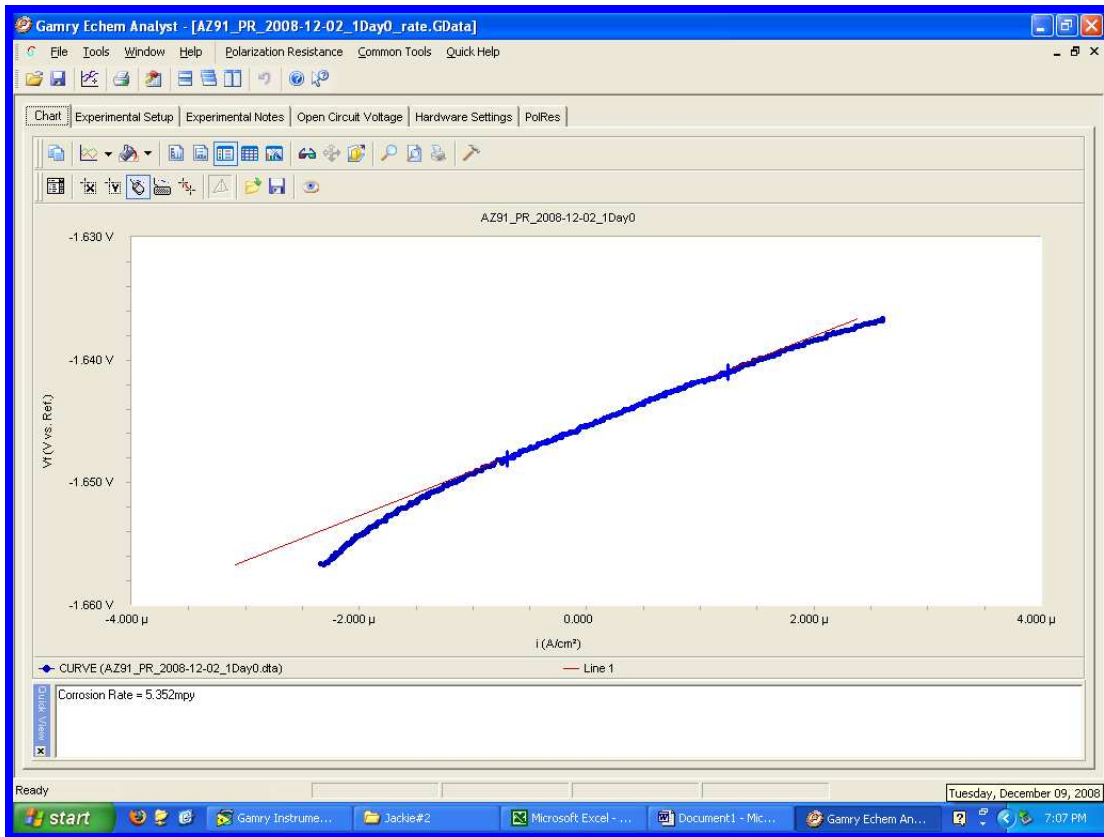


Figure 5. Computer Screen Shot of Polarization Resistance Graph.

A numerical fit of the polarization curve yields a value for the slope of the curve where the current equals zero, which is defined as the polarization resistance (R_p). Ideally, the voltage will equal the open circuit potential of the cell when the current equals zero and the graphed data will be nearly linear in this region. The polarization resistance value is inversely proportional to the corrosion rate and can be used with the values for certain properties of the alloy to calculate the corrosion rate.

3.5 Testing Parameters

The testing parameters were adjusted within Gamry Framework which is the electrochemical experiment software that interfaced with the potentiostat. For

polarization resistance tests, important experimental parameters that were established included the potential range to be scanned, the scan rate, the sample period, and the initial delay to reach open circuit potential. The range to be scanned was set with respect to the open circuit potential of the corrosion cell or E_{oc} . The selected scan range was from 10 mV below E_{oc} to 10 mV above E_{oc} . The scan rate was 0.2 mV/s and the sample period was 0.2 seconds. The initial delay was set for between 100 to 300 seconds to allow for the system to reach a stable open circuit potential. The initial delay was manually extended if the system required additional time to reach a stable open circuit potential. Figure 6 shows a computer screen shot of the window in Gamry Framework displaying the testing parameters of the experimental setup.

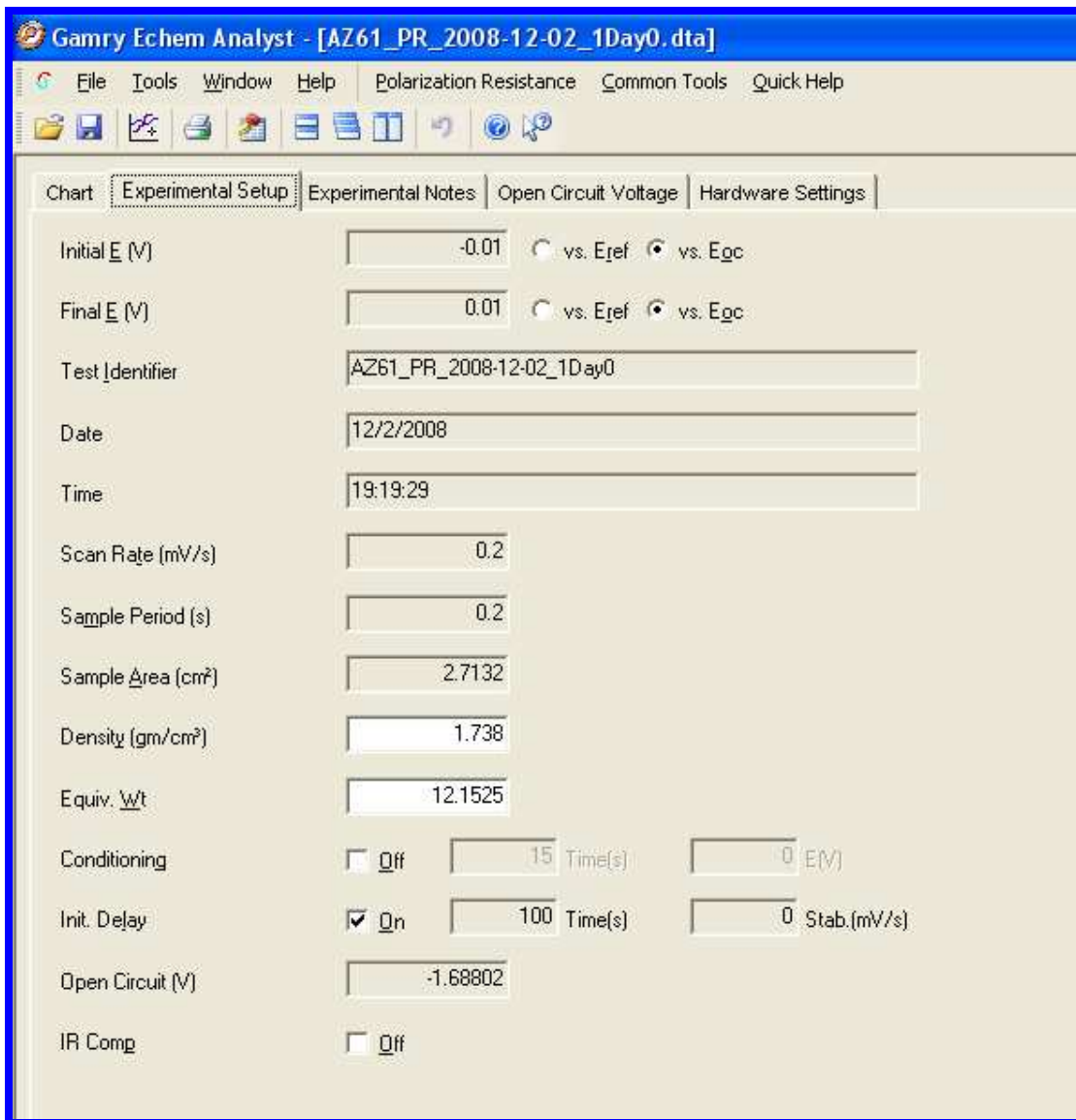


Figure 6. Experimental Setup Window for Polarization Resistance in Gamry Framework.

Chapter 4 – Results and Discussion

4.1 Corrosion Rate Data

The polarization resistance experiments provided polarization resistance, R_p , values for the samples while immersed in HBSS over time. The R_p was used to calculate the i_{corr} value which is the corrosion rate in microamperes per square centimeter. R_p to i_{corr} are inversely proportional with a proportionality constant B as shown by the equation below.

$$i_{corr} = \frac{B}{R_p} \quad (1)$$

The proportionality constant is defined with respect to two Tafel constants, β_a and β_c .

$$B = \frac{\beta_a \beta_c}{2.3 \cdot R_p \cdot (\beta_a + \beta_c)} \quad (2)$$

$$\beta_a \approx \beta_c \approx 0.1V \quad (3)$$

The Tafel constants are approximated to be 0.1 volts as this value has been shown to produce a constant error in calculated corrosion rate of only a factor of two maximum. The i_{corr} value obtained through the relationship above is in amperes per centimeter square as shown by the dimensional analysis below.

$$\frac{V^2}{\Omega \cdot cm^2 \cdot V} = \frac{V}{\Omega \cdot cm^2} = \frac{A}{cm^2} \quad (4)$$

A sample calculation for the i_{corr} value when the R_p was $484.5 \Omega \cdot cm^2$ is shown below.

$$i_{corr} = \frac{0.1V \cdot 0.1V}{2.3 \cdot 484.5 \Omega \cdot cm^2 \cdot (0.1V + 0.1V)} = 37.19 \frac{\mu A}{cm^2} \quad (5)$$

The i_{corr} value can then be converted to the corrosion rate in mils per year (mpy) which is the equivalent of 0.001 inches per year using the following equation where R_{mpy} is the corrosion rate in mils per year, a is the atomic weight in grams, n is the number of equivalents exchanged, and D is the sample density in grams per centimeter cubed. A sample calculation for R_{mpy} is also shown below.

$$R_{mpy} = 0.129 \frac{a \cdot i_{corr}}{n \cdot D} \quad (6)$$

$$R_{mpy} = 0.129 \cdot 12.39g \frac{37.19 \frac{\mu A}{cm^2}}{1.78 \frac{g}{cm^2}} = 33.40 mpy \quad (7)$$

The corrosion rate data obtained from preliminary experiments with AZ31, AZ61, and AZ91 is shown in the table below. Two replicate samples of each bulk material were tested at during each test. Two tests were performed at different times on AZ61 and AZ91 and one test was performed on AZ31 at the same time as the second tests for AZ 61 and AZ91. If polarization resistance testing was not performed on a particular day, this is indicated by “n/a” in the chart.

Immersion Time (Days)	Corrosion Rate (mpy)									
	AZ31 Sample 1	AZ31 Sample 2	AZ61 Test 1 Sample 1	AZ61 Test 1 Sample 2	AZ61 Test 2 Sample 1	AZ 61 Test 2 Sample 2	AZ91 Test 1 Sample 1	AZ 91 Test 1 Sample 2	AZ91 Test 2 Sample 1	AZ 91 Test 2 Sample 2
0	10.49	12.87	82.13	44.73	14.77	11.55	2.703	1.504	5.352	6.101
1	20.51	22.91	6.68	0.5549	32.05	30.3	3.066	1.533	3.401	22.7
2	29.94	31.69	72.44	42.09	27.37	27.05	6.132	8.915	8.725	22.33
3	21.11	29.95	39.05	0.2669	22.25	29.71	5.848	3.789	7.706	8.378
4	32.72	28.1	49.1	0.4531	31.45	39.07	1.087	1.819	7.237	7.863
5	56.45	41.3	25.86	0.3037	38.15	47.77	2.697	1.524	9.35	10.47
6	33.92	32.24	29.13	9.453	21.16	23.07	2.672	1.561	5.241	10.92
7	41.1	34.32	23.24	2.391	18.26	35.64	1.717	1.677	4.653	10.48
10	50.69	49.61	10.79	1.904	16.74	54.69	1.045	2.851	5.243	9.17
13	45.35	26.59	4.59	0.8495	n/a	n/a	2.131	3.241	n/a	n/a
14	33.59	47.85	n/a	n/a	27.53	19.35	n/a	n/a	11.32	16.24
16	n/a	n/a	14.54	1.547	33.62	21.91	n/a	n/a	6.31	16.08
19	n/a	n/a	n/a	n/a	n/a	n/a	6.11	5.497	n/a	n/a
22	n/a	n/a	7.199	2.673	n/a	n/a	1.95	5.083	n/a	n/a
25	n/a	n/a	7.791	1.839	n/a	n/a	2.707	6.197	n/a	n/a
28	n/a	n/a	16.6	1.823	n/a	n/a	1.869	10.82	n/a	n/a

Table 5. Corrosion Rate Data for AZ Samples in HBSS over Time.

The corrosion rate data for the primary experiments with the non equilibrium vapor deposited thin and thick film alloys are shown in the tables below.

Sample	Density (g/cm ³)	Equivalent Weight (g)	Time (hr)	R _p (Ω*cm ²)	I _{corr} (μA/cm ²)	mpy
Mg 87w	1.85	12.77	0	2594	8.38	7.46
			2.35	1504	14.45	12.87
			3.53	1418	15.33	13.65
Mg 89x	1.97	13.43	0	8386	2.59	2.28
			1.9	6442	3.37	2.97
			3.77	8146	2.67	2.35
			5.72	3675	5.92	5.20
Mg 91w	1.90	13.01	0	860.1	25.28	22.33
			3.2	1044	20.82	18.39
			5.1	757.8	28.69	25.34

Table 6. Corrosion Rate Data for Thin Film Samples in HBSS over Time.

Sample	Density (g/cm ³)	Equivalent Weight (g)	Time (hr)	R _p (Ω*cm ²)	I _{corr} (μA/cm ²)	mpy
Thk1w	1.75	12.22	0	358.4	60.66	54.64
			2.03	380.2	57.18	51.51
			4	382	56.91	51.26
			6	390.3	55.70	50.17
			8	343.6	63.27	56.99
Thk1x			0	288.8	75.27	67.81
			2.13	280.9	77.39	69.71
			4	513.9	42.30	38.11
			6	411.5	52.83	47.59
			8	332.9	65.30	58.82
			10.02	359.8	60.42	54.43
			11.73	354	61.41	55.32
			12.7	385.8	56.35	50.76
			13.45	348.1	62.45	56.25
			14.4	257.6	84.39	76.02
Thk15w	1.78	12.39	0	584.5	37.19	33.40
			2.02	428.9	50.69	45.51
			3.95	222.5	97.70	87.73
			6	113.4	191.70	172.14
			8	87.73	247.80	222.50
			10.08	99.34	218.84	196.50
			11.95	109.2	199.08	178.76
			12.92	108.1	201.10	180.57
			13.88	104.7	207.63	186.44
			14.88	93.46	232.60	208.86
Thk15x			0	297.8	73.00	65.55
			1.92	417.6	52.06	46.74
			4.02	253.2	85.86	77.09
			6.03	356	61.06	54.83
			8.1	166.8	130.33	117.03

Table 7. Corrosion Rate Data for Thick Film Samples in HBSS over Time.

4.2 Experimental Analysis

The corrosion rates of the two samples for each test were averaged and graphed versus the immersion time in hours. Below is the graph for the primary experiments. The corrosion rates of AZ91 were consistently lower than either AZ61 or AZ31.

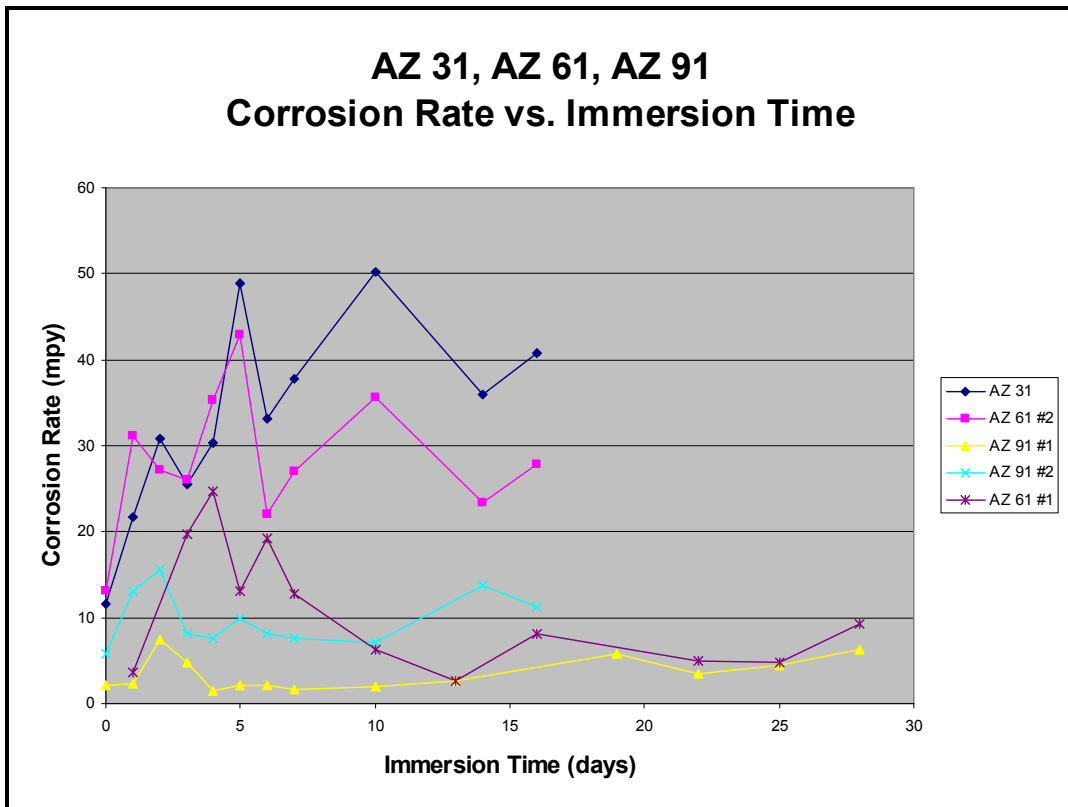


Figure 7. Graph of Corrosion Rate vs. Immersion Time for Averaged Tests Values for Each Sample Type.

Below are the graphs of corrosion rate versus immersion time for the primary experiments. The thin film samples graph is shown first and followed by the graph for the thick film samples.

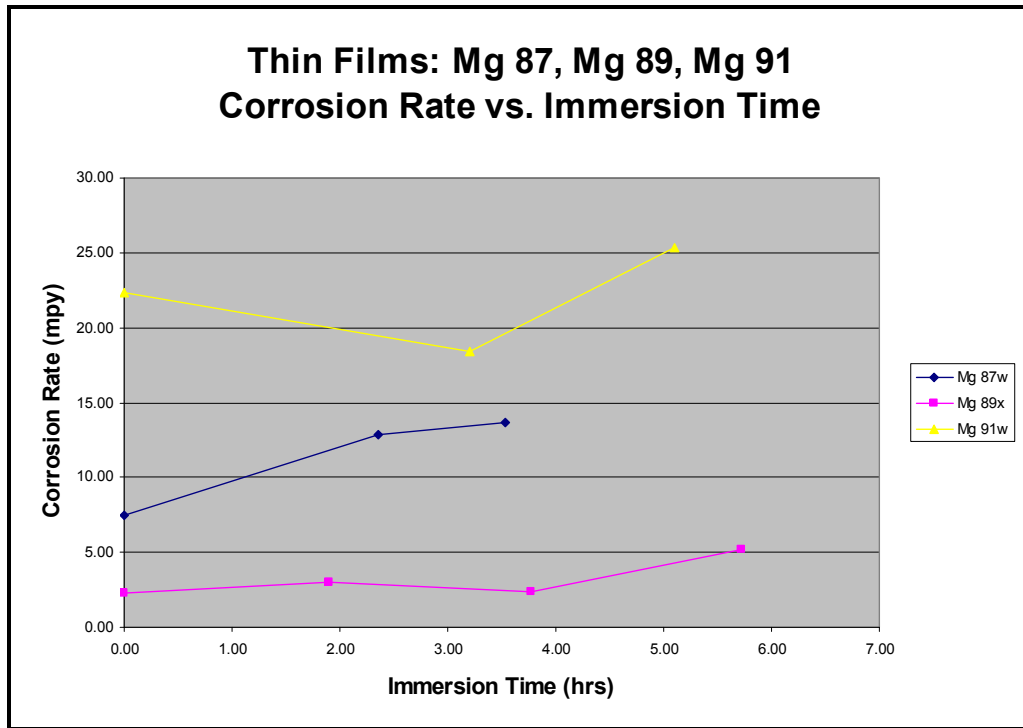


Figure 8. Graph of Corrosion Rate vs. Immersion Time for Averaged Tests Values for Each Thin Film Sample Type.

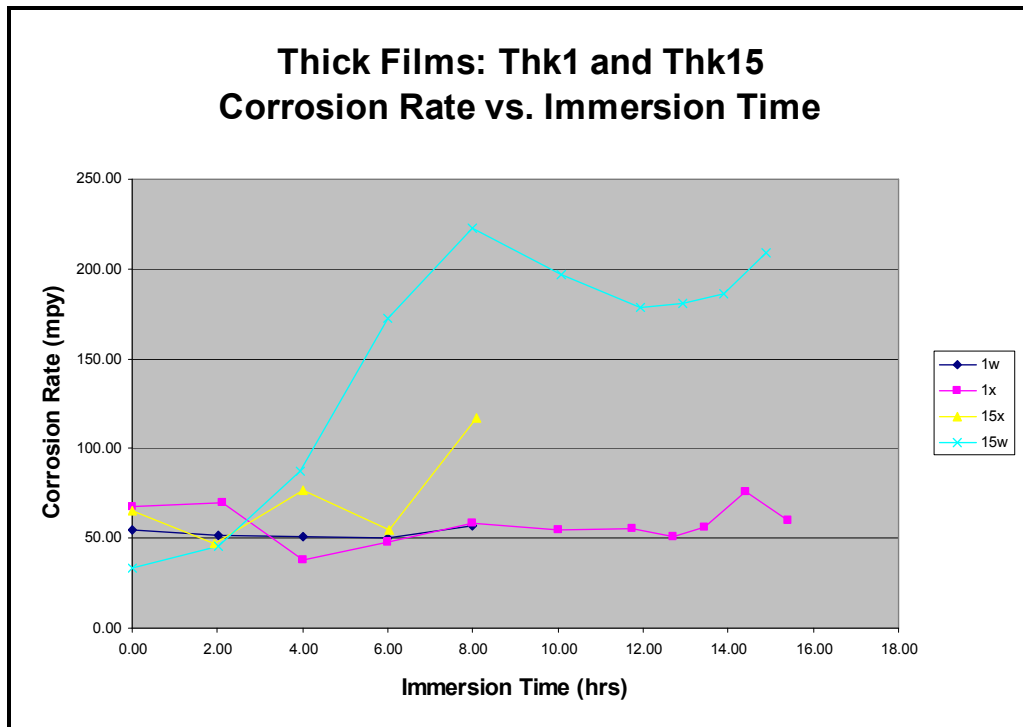


Figure 9. Graph of Corrosion Rate vs. Immersion Time for Averaged Tests Values for Each Thick Film Sample Type.

4.3 Surface Photographs

Photographs of the surfaces of the samples were taken before and after testing. The photographs are essential in order to provide insight into the type of corrosion that occurred and the size and kind of corrosion products that formed. The photographs below compare the surfaces of some of the samples before and after the completion of the polarization resistance and electrochemical impedance spectroscopy tests performed. Analyzing the surface changes during corrosion of a material being considered for use in a bioabsorbable cardiac stent or other biomaterial is important. Ideally, the material would corrode uniformly eliminating the possibility that large pieces of corrosion product break free and pose health risks to the patient. Additionally, localized corrosion may weaken the mechanical properties of the material before the biomaterial has completely performed its function thereby negating much of the benefit of the device.

All of the photo comparisons show visible buildup of corrosion products on the sample surface after testing. Observation of the samples surfaces before testing shows distinct differences in the surfaces between the types of samples. The bulk material sample in Figure 10 appears to have a much rougher surface than any of the thin or thick film samples in the other figures.



Figure 10. Surface images of AZ61 before testing (left) and after 28 days of immersion and testing in HBSS (right).

Visually, both the initial and final sample surfaces of the thin film samples in Figure 11 and Figure 12 appear to be quite similar suggesting that the deposition method produces consistent results and that the corrosion occurred in a similar manner on both samples.



Figure 11. Surface images of Mg 87w before testing (left) and after immersion and testing in HBSS (right).

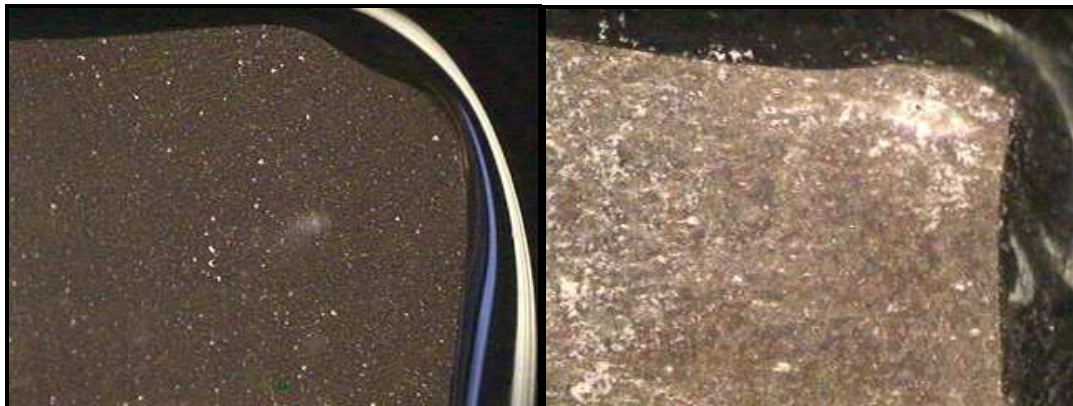


Figure 12. Surface images of Mg 91w before testing (left) and after immersion and testing in HBSS (right).

A white powdery corrosion product is present on both of the thick film samples shown below. In Figure 13, there is an increased buildup of corrosion products near the upper edge of the sample. However, the sample in Figure 14 experienced more significant corrosion near the middle of the sample where the sample appears to have fractured as a result of the corrosion.



Figure 13. Surface images of Thk1w before testing (left) and after immersion and testing in HBSS (right).

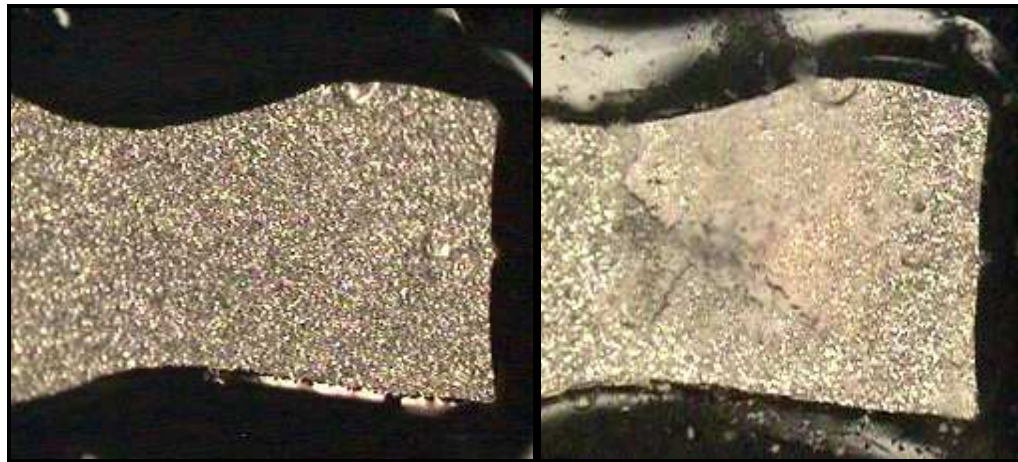


Figure 14. Surface images of Thk15x before testing (left) and after immersion and testing in HBSS (right).

Under the microscope, surface defects were identified on some of the samples as seen in the photographs below. These surface defects may have influenced the corrosion rate and the length of time in which the sample could be tested.

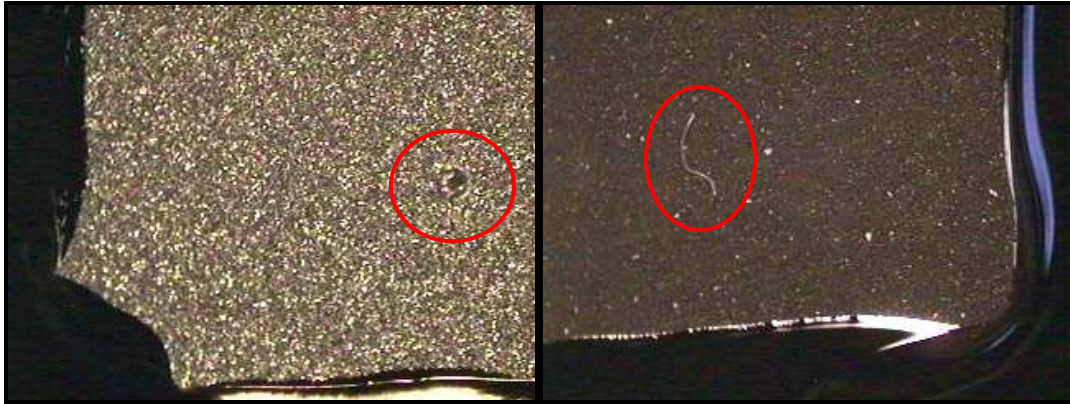


Figure 15. Images of the surfaces of two samples before testing reveal the presence of surface defects highlighted in these images by the surrounding red ovals.

4.4 Interpretation

- 1) In general, the corrosion rate of the AZ alloy samples decreased over time as a film of the corrosion products builds up on the surface of the sample forming a protective layer.
- 2) AZ91 showed a distinctly lower corrosion rate than AZ61 and AZ31. This result is due to the higher concentration of aluminum in the AZ91 alloy since aluminum is a more corrosion resistant and less reactive element than magnesium.
- 3) The thick film samples lasted considerably longer than the thin film samples of alloys of similar composition. This can be attributed to the

difference in thickness from 2-3 micrometers for the thin films to about 300 micrometers for the thick films.

- 4) The non equilibrium vapor deposited magnesium alloys exhibited different corrosion performance between not only samples of varying composition but also between different samples of the same composition. The corrosion rate ranges as well as the corrosion rate trends over time were not consistent. This type of variation in results is not unusual for magnesium alloys. These results emphasize the multitude of factors that can affect corrosion rate including all of the following:
 - a. Alloy composition
 - b. Surface defects
 - c. Storage time in desiccators
 - d. Deposition parameters
 - e. Processing
 - f. Microstructure and morphology (atom structure, density, defects, etc.)

Chapter 5

Conclusions

5.1 Summary

Electrochemical experiments were performed on magnesium alloys including bulk samples of conventionally processed AZ31, AZ61, and AZ91 as well as on thin and thick film samples of experimental non equilibrium vapor deposited alloys. The vapor deposited magnesium samples were alloyed with titanium and yttrium and are being studied as possible materials for use in bioabsorbable cardiac stents. The AZ series of alloys has already been identified as having corrosion properties similar to those desired in bioabsorbable cardiac stents. The aluminum in these alloys increases the corrosion resistance of magnesium which is extremely reactive and easily corroded. However, there is speculation as to whether aluminum will present any health concerns in the human body. The vapor deposition method of fabrication allows for a greater amount of alloying material to be incorporated into the alloy by extending the soluble limits of the alloying components. Ideally, this will allow the corrosion resistance of the magnesium alloys to be increased without the use of aluminum. Results indicated that there was substantial variation in corrosion rates of the thin and thick film samples due to factors beyond just alloy composition including surface defects, storage time in desiccators, deposition parameters, processing, and microstructure and morphology. Hopefully, by determining the effects of composition and other factors on the corrosion properties of the non equilibrium vapor deposited

alloys, an alloy with properties ideal for use in a bioabsorbable cardiac stents can be designed.

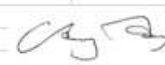
5.2 Future Work Suggestions

There are many opportunities for further research on magnesium alloys to better determine their potential as a biomedical implant material. A better understanding of their corrosion process will allow aid in the design of the material to corrode at the desired rate and in the desired manner within the human body. Similar experiments to those detailed in Chapter 3 should be repeated with additional non equilibrium vapor deposited magnesium alloys to ensure that the results are consistent and to develop a deeper understanding of how the varying alloy compositions affect the type and rate of corrosion experienced by the samples. Furthermore, there are limitations to performing *in vitro* testing on the materials and *in vivo* testing will be the only way to truly evaluate the body's response to the alloys and the alloys response to the environment within the human body.

Appendix A – Tools

Computer software was used extensively to aid in data collection and analysis throughout the project. The primary software applications used were Gamry Instruments software and Motic Images software. The potentiostat interfaced with the computer through Gamry Instruments software. Electrochemical experiments including both polarization resistance and electrochemical impedance spectroscopy were performed in Gamry Framework and the results were analyzed using Gamry Echem Analyst. Motic Images was the software connected to the microscope and was used to capture still surface photos of the samples before and after testing. Additionally, Motic Images was used to determine the surface area of the thin and thick film samples by calibrating the microscope and then tracing and calculating the area of the film using the software.

Appendix B – Alloy Composition Analyses

 PENNSTATE Materials Characterization Lab		Materials Research Institute Henry Gong Senior Analytical Chemist 312 Hosler Building The Pennsylvania State University University Park, PA 16801-4801 hrg2@psu.edu, 814 865-1981, Fax 814 865-8094							
April 24, 2008									
From: Henry Gong, 312 Hosler Bldg. 312 Hosler Building University Park, PA 16802									
To: Nicholas Pytel									
Subj: Spectrochemical Characterization of solutions									
Our #	08-0755	08-0756	08-0757	08-0758	08-0759	08-0760	08-0761	08-0762	
Your #	alfa	usmg	a231	a261	a291	hbss1	hbss2	hbss3	
Al (ppm)	0.25	0.42	21	65	130	0.23	0.24	0.21	
Cu (ppm)	0.03	0.04	0.02	0.02	0.02	0.15	0.05	0.03	
Fe (ppm)	0.11	0.41	0.09	0.23	0.14	0.04	0.05	0.04	
K (ppm)	0.27	0.33	0.29	0.32	0.38	< 01	< 01	< 01	
Mg (ppm)	900	1150	685	1050	1350	18	17	18	
Mn (ppm)	0.01	0.03	2.1	2.7	2.8	< 01	< 01	< 01	
Na (ppm)	2.1	2.9	2.2	2	2.6	2300	2300	2250	
Ni (ppm)	< 01	< 01	< 01	< 01	< 01	< 01	< 01	< 01	
Pb (ppm)	< 01	< 01	0.01	0.04	0.05	< 01	< 01	< 01	
Sn (ppm)	< 01	< 01	< 01	< 01	< 01	< 01	< 01	< 01	
Zn (ppm)	0.09	0.07	7.4	6.9	9.8	0.03	0.02	0.02	
Our #	08-0763	08-0764	08-0765	08-0766	08-0767	08-0768	08-0769	08-0770	
Your #	a1	a2	a3	a4	a5	mgextra aa	mgextra bb	mgextra x1	
Mg (ppm)	8.4	27	34	87	67	150	170	420	
Ti (ppm)	0.18	1.0	1.7	3.9	2.3	2.3	2.7	13	
Y (ppm)	0.30	2.0	3.0	5.4	3.6	16	19	7.6	
Note:									
Results in parts per million (by weight) on as-received basis									
Samples were run on a Perkin-Elmer Optima 5300 ICP (inductively coupled plasma emission spectrometer) Synthetic standards from High Purity Standards were used to calibrate the results.									
									

From: Henry Gong
 312 Hoster Building
 University Park, PA 16802
 To: John D. Petrilli

Subj: Spectrochemical Characterization of solution

Our #	09-0440	09-0441	09-0442	09-0443	09-0444	09-0445	09-0446	09-0447	09-0448	09-0449
Your #	1	3	15	16	33	54	80	84	88	89
Al (ppm)	0.26	0.26	0.29	0.23	0.28	0.15	0.26	0.22	0.25	0.18
Ca (ppm)	0.12	0.28	0.16	0.19	0.09	0.05	0.06	0.65	0.65	0.72
Cu (ppm)	< .01	< .01	< .01	< .01	0.02	< .01	< .01	0.02	< .01	< .01
Fe (ppm)	0.16	0.07	0.05	0.04	0.02	0.02	0.02	0.03	0.02	0.02
K (ppm)	0.27	0.28	0.26	0.25	0.21	0.18	0.20	0.23	0.24	0.23
Mg (ppm)	105.00	140.00	105.00	73.10	11.50	1.47	9.09	53.70	70.00	63.10
Mn (ppm)	< .01	< .01	< .01	< .01	< .01	< .01	< .01	< .01	< .01	< .01
Na (ppm)	< .01	< .01	< .01	< .01	< .01	< .01	< .01	< .01	< .01	< .01
Ni (ppm)	< .01	< .01	< .01	< .01	0.02	< .01	< .01	< .01	< .01	< .01
Si (ppm)	1.01	0.92	1.01	0.99	1.01	0.74	0.99	1.01	1.00	0.81
Ti (ppm)	0.19	0.61	0.38	0.41	< .01	< .01	0.16	< .01	2.91	2.92
Zn (ppm)	< .01	< .01	< .01	< .01	< .01	< .01	< .01	< .01	< .01	< .01
Y (ppm)	1.19	4.33	2.68	2.83	1.08	0.69	0.94	12.60	12.80	13.60
Sum(Mg,Y,Ti)	106	145	108	76	13	2	10	66	86	80
Your #	1	3	15	16	33	54	80	84	88	89
Al (ppm)										
Ca (ppm)										
Cu (ppm)										
Fe (ppm)										
K (ppm)										
Mg (ppm)	98.70	96.59	97.17	95.76	91.41	68.06	89.21	81.00	81.67	79.25
Mn (ppm)										
Na (ppm)										
Ni (ppm)										
Si (ppm)										
Ti (ppm)	0.18	0.42	0.35	0.54			1.57		3.40	3.67
Zn (ppm)										
Y (ppm)	1.12	2.99	2.48	3.71	8.59	31.94	9.22	19.00	14.93	17.08

Note:

Results in parts per million (by weight) on as-received basis

Samples were run on a Perkin-Elmer Optima 5300 ICP (inductively coupled plasma emission spectrometer) Synthetic standards from High Purity Standards were used to calibrate the results.



January 30, 2009

From: Henry Gong
312 Hosler Building
University Park, PA 16802
To: John D. Petrilli

Subj: Spectrochemical Characterization of solution

	Our #	09-0124		09-0151		09-0449		09-0152					
	Your #	0	P 0 ?	87	p 87 ^r	89 ^r	89	91	p 91				
Al (ppm)		0.26		0.11		0.17		0.18		0.20			
Ca (ppm)		0.03		0.34		1.07		0.48		0.28	0.72	0.15	
Cu (ppm)		< .01		0.39		0.02		< 01		0.02	< .01	< 01	
Fe (ppm)		0.01		0.02		<0.02		0.01		0.01	0.02	0.01	
K (ppm)		0.22		0.32		0.21		0.25		0.19	0.23	0.23	
Mg (ppm)		0.05		0.14		178.00		86.00		25.00	63.10	53.00	21.30
Mn (ppm)		< 01		<0.02		< 01		< 01		< .01	< .01	< 01	
Na (ppm)		1.40		4.50		1.48		2.84		1.50	< .01	3.16	
Ni (ppm)		< .01		< 01		<0.02		< 01		< .01	< .01	< 01	
Si (ppm)		0.44		0.82		0.20		0.68		0.42	0.81	0.69	
Ti (ppm)		< .01		< 01		3.27		1.61		1.00	2.92	1.60	0.62
Y (ppm)		< .01				16.24		8.00		5.00	13.60	6.90	2.67
Zn (ppm)		< 01				0.08		< 01		< .01	< .01	< 01	
Mg(p) / Mg						0.48						0.40	
Ti(p) / Ti						0.49						0.39	
	Your #	0	P 0	87	p 87 ^r	89 ^r	89	91	p 91				
Sum of ppm				197.51	95.61	31.00	79.62	61.50	24.59				
Weight Percent	Fe												
	Mg			90.12	89.95	80.65	79.25	86.18	86.61				
	Ti			1.66	1.68	3.23	3.67	2.60	2.52				
	Y			8.22	8.36	16.13	17.08	11.22	10.87				
Ratio Y / Ti				4.97	4.97	5.00	4.66	4.31	4.31				

Note: *missing Y content calculated by multiplying Y * Ti(p) / Ti
*Fe content in TFs appears to be from tweezer contamination

Results in parts per million (by weight) on as-received basis

Samples were run on a Perkin-Elmer Optima 5300 ICP (inductively coupled plasma emission spectrometer) Synthetic standards from High Purity Standards were used to calibrate the results.

	Your #	0	P 0	87	p 87 ^r	89 ^r	89	91	p 91
Atomic Percent	Mg			96.69	96.63	93.02	92.39	95.15	95.32
	Ti			0.90	0.92	1.89	2.17	1.46	1.41
	Y			2.41	2.46	5.09	5.44	3.39	3.27

References

- Dvorak, Paul. "Ideas and lasers build better stents." Medical Design News 1 Oct. 2008: 51-55.
- Erne, Paul, Matthias Schier, and Therese J. Resink. "The road to bioabsorbable stents: reaching clinical reality?" CardioVascular and Interventional Radiology 29 (2006): 11-16.
- Hansen, Douglas C. "Metal corrosion in the human body: the ultimate bio-corrosion scenario." The Electrochemical Society Interface 17 (2008): 31-34.
- Hiromoto, Sachiko. "Corrosion of metallic biomaterials in cell culture environments." The Electrochemical Society Interface 17 (2008): 41-44.
- Jones, Denny A. Principles and Prevention of Corrosion. 2nd ed. Upper Saddle River: Pearson plc, 1996.
- Levesque, Julie, Hendra Hermawan, Dominique Dube, and Diego Mantovani. "Design of a pseudo-physiological test bench specific to the development of biodegradable metallic biomaterials." Acta Materialia 4 (2008): 284-95.
- Schmutz, Patrik, Ngoc-Chang Quach-Vu, and Isabel Gerber. "Metallic medical implants: electrochemical characterization of corrosion processes." The Electrochemical Society Interface 17 (2008): 35-40.
- Shaw, Barbara A., Elizabeth Sikora, and Sanna Virtanen. "Fix, heal, and disappear: a new approach to using metals in the human body." The Electrochemical Society Interface 17 (2008): 45-49.
- Song, Guangling, and Andrej Atrens. "Understanding magnesium corrosion: a framework for improved alloy performance." Advanced Engineering Materials 5 (2003): 837-58.
- Song, Guangling, and Andrej Atrens. "Corrosion mechanisms of magnesium alloys." Advanced Engineering Materials 1 (1999): 11-33.
- Song, Guangling. "Recent progress in corrosion and protection of magnesium alloys." Advanced Engineering Materials 7 (2005): 563-86.
- Staiger, Mark P., Alexis M. Pietak, Jerawala Huadmai, and George Dias. "Magnesium and its alloys as orthopedic biomaterials: a review." Biomaterials 27 (2006): 1728-734.

Waksman, Ron, Rajbabu Pakala, Teruo Okabe, David Hellinga, Rosanna Chan, Min O. Tio, Eric Wittchow, Sonja Hartwig, Karl-Heinz Waldmann, and Claus Harder. "Efficacy and safety of absorbable metallic stents with adjunct intracoronary beta radiation." Journal of Interventional Cardiology 20 (2007): 367-72.

ACADEMIC VITA of Jacqueline G. Van Pelt

150 Farm Valley Road
Wellsville, PA 17365
jgv116@psu.edu

EDUCATION

Bachelor of Science in Engineering Science with Honors
The Pennsylvania State University
December 2009

Honors in Engineering Science, Schreyer Honors College

Thesis Title:

Magnesium Alloys for use in Bioabsorbable Cardiac Stents

Thesis Supervisor: Dr. Barbara A. Shaw

Licensing: Engineer in Training (EIT)

PROFESSIONAL EXPERIENCE

Engineering and Advanced Support Technology, Inc.
Wellsville, PA

May 2004 - present

Engineering Aide – assisting with design documentation and proposal development, organizing and facilitating design collaboration, developing integrated master schedules for defense contracts ranging from \$100,000 engineering change proposals to \$3.5 million multi-year contracts, and working with graphic design professionals to create powerful and meaningful visual aids

Capstone Research and Design Project and Thesis

University Park, PA

August 2008 – May 2009

Magnesium Alloys for use in Bioabsorbable Cardiac Stents

Research and Thesis Candidate – investigating design options and identifying design solutions, recording impressions and progress, designing experiments and tests, interpreting results, and writing literature reviews and research reports

Penn State Cooperative Extension of Adams County

Gettysburg, PA

Summer 2006

Engineering Intern – equipment development, design, testing, modification, and implementation; applying mechanical problem solving and technical writing skills; collaborating with others and working within a multidisciplinary team

**OTHER
EXPERIENCE**

Penn State University Ambulance Service

December 2006 – present

Ambulance Crew and Event Staff Emergency Medical
Technician

Assistant Instructor, Kinesiology 403 – Emergency
Medical Technology

Pennsylvania Department of Health

May 2009 – present

Certified Emergency Medical Services Instructor

Penn State Residence Life

August 2006 – May 2009

Community Assistant in University Apartments and Suites
Resident Assistant in South Area Residence Halls

Gifford Pinchot State Park

Summers 2005 and 2006

Lifeguard

HONORS / AWARDS

- Best Design Communication Award, BAE Engineering Project
- National Residence Hall Honorary Inductee, Nittany Chapter
- Dean's List – Fall 2005, Spring 2006, Fall 2006, Fall 2007, Spring 2008, Fall 2008

**COMMUNITY
INVOLVEMENT**

- Pleasant Gap Fire Department Live-In Volunteer
Emergency Medical Technician
- 4-H Club Screened Volunteer and Bylaw Review
Committee Facilitator
- Honors Chemistry Lab Project – Lead Paint Analysis
of PSU Buildings
- Penn State Club Field Hockey